

Analytical fibre bundle model to investigate the roles of fracture mechanics and dynamic stresses during the longitudinal tensile failure in fibre-reinforced composites

Jorge Moledo Lamela*, Gianmaria Bullegas[†] and Silvestre T. Pinho[‡]
Imperial College London, South Kensington Campus, SW7 2AZ London, United Kingdom

A semi-analytical Monte Carlo fibre bundle model was developed to investigate the role of dynamic effects and fracture mechanics in the longitudinal tensile failure of fibre-reinforced composites. To the knowledge of the authors, it is the first time that both effects are implemented in a fibre bundle model through direct simulation. The formulation includes a field superposition method to calculate the stress concentration around broken fibres which captures the effect of clusters of broken fibres. The Monte Carlo process was optimized to allow the simulation of bundles with thousands of fibres. The comparison between the predicted bundle strengths and experimental data suggests that, although the dynamic stress concentration significantly decreases the bundle strength, the trend and magnitude of the size effects in large composite bundles can only be explained considering fracture mechanics as the failure mechanism.

I. Introduction

Composite materials, especially Fibre Reinforced Plastics (FRPs), have changed the aeronautical industry since their relatively recent introduction in aircraft structures. Future investigation in this field, with the development of reliable mechanical models, seem key for an industry where both mechanical performance and weight are critical factors.

The strength and stiffness of FRP laminates is controlled, to a great extent, by the fibres in the load-aligned plies, thus fibre-dominated tensile failures can lead to a significant drop in local stiffness, and can trigger catastrophic failure of an entire composite structure. The longitudinal tensile strength of unidirectional (UD) FRPs is characterized by strong size effects connected to both the length of the specimens and the total number of fibres.¹⁻⁴ Since the formation of clusters of broken fibres and their catastrophically propagation once reached a critical size govern the longitudinal tensile failure, larger structures (with more and/or longer fibres than a smaller one) will be more likely to have more defects, making easier the formation of a critical cluster of broken fibres and lowering the final strength.

The stochastic variability of the single fibre strength and the stress redistribution that occurs around broken fibres have been identified as important factors to predict size effects.⁵⁻⁸ Several Fibre Bundle Models (FBMs) created in the literature aim to predict the stress concentrations generated in the intact fibres after fibre failures in a bundle remotely loaded under tension.⁶ In these FBMs, this load is progressively increased until all fibres are broken, or until the composite cannot withstand further load increments, in order to predict the strength of the bundle.

Some analytical FBMs were developed,^{9,10} and Pimenta and Pinho recently proposed an analytical hierarchical scaling law for the strength of composite bundles which has been validated against experimental results.^{6,11} Nevertheless, in most models in the literature the ultimate strength of the bundle is a stochastic variable which has to be characterized statistically through Monte Carlo simulations.⁵ These Monte Carlo FBMs calculate stress fields around broken fibres through Finite Elements (FE)¹²⁻¹⁵ or combined field-superposition methods,^{7,8,16} which calculate deterministic stress fields near single-fibre breaks and then use a superposition method to include those fields in the failure simulation of fibre bundles with multiple breaks.

However, most FBMs only consider fibre stress overload (i.e. strength of materials approach) as the bundle failure criterion, thus failing to predict size effects accurately.^{12,14} Bazant has shown that final failure of a composite structure is governed by the composite fracture toughness for large-scale components,¹⁷ and there is growing experimental evidence that unstable failure of carbon fibre/polymer matrix bundles occurs when a cluster of approximately 14 or

*MSc in Aeronautical Engineering, School of Aeronautical and Space Engineering, Universidad Politécnica de Madrid, Plaza Cardenal Cisneros 3, 28040, Madrid.

[†]Faculty member, Supervisor, Department of Aeronautics, Imperial College London, South Kensington Campus, SW7 2AZ London, UK.

[‡]Faculty member, Supervisor, Department of Aeronautics, Imperial College London, South Kensington Campus, SW7 2AZ London, UK.

more broken fibres is formed.^{18,19} Furthermore, fibre failure is a dynamic process, resulting in a change of stress field over time, before it finally dampens to the static level. Dynamic stress concentrations can be significantly higher than static ones,⁹ but all state-of-art FMBs ignore this effect and only consider static equilibrium stress states.²⁰

This paper presents the development of a Monte Carlo FBM with a semi-analytical field superposition method that implements both the effects of dynamic stress concentrations and fracture mechanics driven growth of clusters in the failure process. In order to allow the direct simulation of large bundle sizes, the Monte Carlo simulation process was optimised using statistical analysis. The work was part of a wider research effort into the statistical characterization of the strength of composite structures. A full description of the model development can be found in Bullegas, Lamela et al.²¹

The paper is organised as follows: Section II presents the theoretical basis of the model, including the formulation of the dynamic effects and fracture mechanics features. Section III contains an overview of the numerical results and a comparison between experimental and predicted strength distributions both in micro and macro-bundles, followed by the discussion in Section IV. Finally, Section V draws the main conclusions.

II. Model development

The geometry considered in the model is a bundle of n_f fibres of length l_s , diameter ϕ_f and cross section A_f with fibre volume fraction V_f (Figure 1). Each fibre in the bundle is subdivided into n_{el} fibre elements of size l_{el} . The fibres are packed in a square arrangement with inter-fibre spacing s , although it has been established that the differences due to fibre arrangement are remarkably small.^{8,22} The bundle is loaded in tension by a remote, asymptotic stress σ_∞ applied to the fibre extremities.

Each fibre element ij belonging to a fibre i ($i = 1, \dots, n_f$) and a cross section j ($j = 1, \dots, n_{el}$) is assigned a stochastic strength X^{ij} following a Weibull distribution (see Appendix A), and stands a stress σ^{ij} . If none of the fibres in the bundle are broken, then $\sigma^{ij} = \sigma_\infty \forall ij$. A fibre breaks if $\sigma^{ij} \geq X^{ij}$ for any of its elements; in this case, for the broken/failed element $\sigma^{(ij)_{fa}} = 0$, whereas the rest of the field σ^{ij} needs to be calculated.

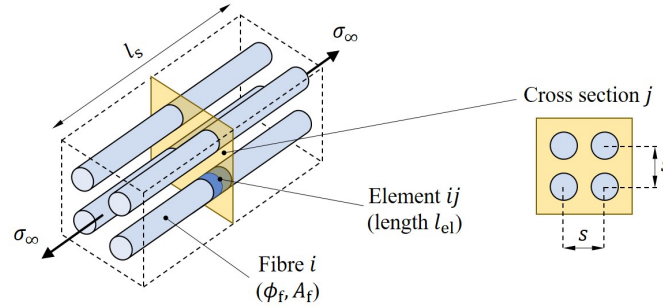


Figure 1 Geometry of the model

A. Shear-lag mechanism and shear-lag stress limit

Once a fibre element fails, the longitudinal stress in that element goes to zero ($\sigma^{(ij)_{fa}} = 0$), but it is recovered in the rest of the fibre due to the shear stress transmitted by the matrix via a shear-lag mechanism^{10,11,23,24} (Figure 2a). This mechanism defines a shear-lag stress limit σ_{sl}^{ij} for each element in the broken fibre, which is the maximum stress level that the element is able to stand.

The portion of the fibre where $\sigma_{sl}^{ij} \leq \sigma_\infty$ is the recovery length associated with the failed element $(ij)_{fa}$, and the elements within it are called *saturated* elements. The non-saturated elements are called *intact* elements. The loss of stress in the saturated elements is redistributed on the rest of the fibres of the bundle, which experience a higher stress concentration in the region of the break (Figure 2b).

Assuming that the axial load is only carried by the fibres, and the matrix is loaded in shear to the yield stress τ_{sl} (perfectly plastic behaviour), the shear-lag stress limit $\sigma_{sl}^{(ij)(ij)_{fa}}$ for each element ij in fibre i due to the failed element $(ij)_{fa}$ can be calculated applying force equilibrium:

$$\sigma_{sl}^{(ij)(ij)_{fa}} = \sum_{i[j-(j)_{fa}]} C_{sl}^{ij} \cdot \frac{\tau_{sl}}{A_f} \cdot l_{el}, \quad (1)$$

where C_{sl}^{ij} is the shear-lag boundary, which is the contour, measured at each cross section j , over which the shear stress is transmitted for each fibre element. Of course, for the broken element $\sigma_{sl}^{(ij)_{fa}(ij)_{fa}} = 0$.

For intact elements, C_{sl}^{ij} is calculated computing the number of interfaces between ij and other intact elements in the cross section j , with a maximum of 4 (see Figure 2c). Note that if a surrounding element is saturated the load transference through this interface is blocked. If there are consecutive saturated elements in the cross section j , they are considered to form a cluster, because the load transmission among them is impeded. If a saturated element ij belongs to a cluster, \mathbb{N}_{cl}^{ij} is the set of elements of the cluster and n_{cl}^{ij} the cluster size. The clusters act as stress lacking-regions, thus C_{sl}^{ij} is the total shear-lag boundary of the cluster divided by the number of elements that contains. Assuming that a single saturated element is a cluster of size 1, a general expression for the shear-lag boundary can be formulated:

$$C_{sl}^{ij} = \frac{C_f}{4} \cdot n_{el,in}^{ij} \quad \text{if } \sigma_{sl}^{ij} > \sigma_\infty \text{ (intact);} \quad C_{sl}^{ij} = \frac{C_f}{4 \cdot n_{cl}^{ij}} \cdot \sum_{\mathbb{N}_{cl}^{ij}} n_{el,in}^{ij} \quad \text{if } \sigma_{sl}^{ij} \leq \sigma_\infty \text{ (saturated)} \quad (2)$$

where C_f is the fibre circumference and $n_{el,in}^{ij}$ is the number of intact elements surrounding element ij . This formulation allows to capture the effect of clusters in the recovery mechanism: attending to Eq.(1), if C_{sl}^{ij} becomes smaller due to the presence of a cluster, then the recovery mechanism is more limited.

Eqs.(1)-(2) are computed twice: first, they are computed without considering the existence of clusters in order to detect the saturated elements, and then applying the correct C_{sl}^{ij} . Extending the formulation to the non-broken fibres and considering the possibility of multiple breaks in the same fibre, the shear-lag stress limit is calculated for all the elements in the bundle:

$$\sigma_{sl}^{ij} = \begin{cases} \infty & \text{if } \nexists (ij)_{fa} \in \text{fibre } i; \\ \min_{[(ij)_{fa}]} \left(\sigma_{sl}^{(ij)_{fa}(ij)_{fa}} \right) & \text{if } \exists (ij)_{fa} \in \text{fibre } i. \end{cases} \quad (3)$$

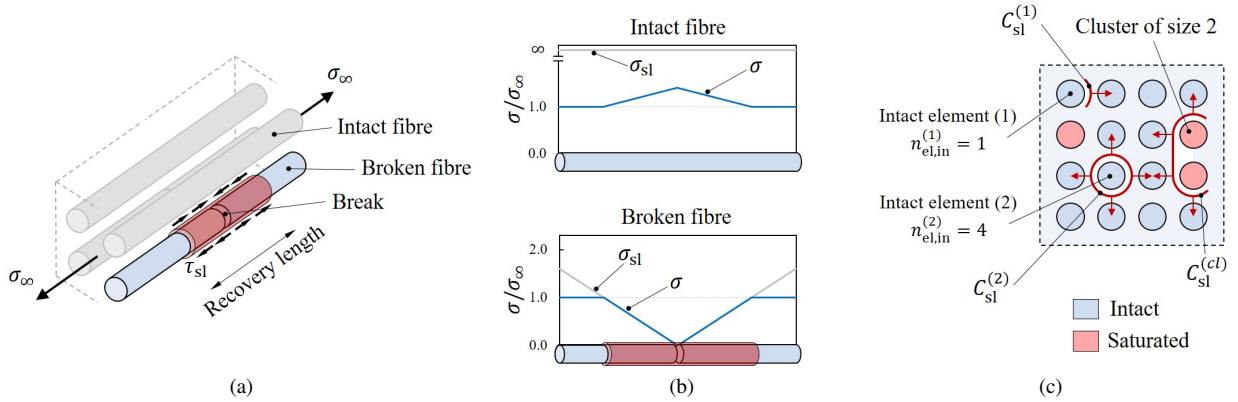


Figure 2 Shear-lag mechanism. (a) Shear-lag mechanism and recovery length definition. (b) Shear-lag stress limit and stress redistribution. (c) Definition of the shear-lag boundary (for two different intact elements and a cluster with two saturated elements; the red arrows indicate the available interfaces for the load transmission).

B. Cluster criticality index

The clusters of broken fibres formed during the damage process may start acting as cracks in the material (Figure 3). If the energy release rate associated with these clusters/cracks is higher than the corresponding fracture toughness of the material, they can trigger catastrophic failure.

Each of the s clusters in each cross section j contains a set \mathbb{N}_{cl}^{sj} of n_{cl}^{sj} saturated elements and can be idealised as an equivalent circular translaminar crack defined by the equivalent diameter a_{eq}^{sj} (see Figure 3b):

$$a_{\text{eq}}^{sj} = \sqrt{\frac{4 \cdot n_{\text{cl}}^{sj} \cdot A_f}{\pi \cdot V_f}}. \quad (4)$$

In order to determine the conditions for the critical propagation of the equivalent crack, an analogy with the problem of a flat penny-shaped crack in an isotropic cylinder is used. In this case, the critical crack size for a given applied stress σ_{eq} depends on the geometry (through a geometrical factor K_g), the material properties (through the Young modulus E and the Poisson ratio ν), the mode I fracture toughness G_{Ic} of the material and the inverse of the square of the stress σ_{eq} .

In the cylinder case, $K_g = \pi/4$ and G_{Ic} is measured for an isotropic material. Nairn^{25,26} developed a shear-lag model that gives estimations for the energy release rate due to crack propagation in unidirectional composites, but it does not apply for clusters of broken fibres. In order to deal with the lack of accurate estimations for G_{Ic} and K_g in composites, a fracture mechanics factor $\lambda_{\text{fm}} [\text{J} \cdot \text{m}^{-2}]$ is introduced. Hence, the critical cluster size a_{cr}^{sj} is

$$a_{\text{cr}}^{sj} = \frac{\lambda_{\text{fm}}}{\sigma_{\text{eq}}^2} \cdot \frac{E}{(1 - \nu^2)}, \quad \text{where } \lambda_{\text{fm}} = K_g \cdot G_{\text{Ic}}. \quad (5)$$

Additionally, it is necessary to consider that (i) the axial load is not carried by the entire cross section but only by the fibres, and (ii) the actual locations of the fibres are not in the same plane, thus stress can still be transferred between the two faces of the equivalent crack due to the friction between the fibres. Hence,

$$\sigma_{\text{eq}}^{sj} = V_f \cdot (\sigma_{\infty} - \sigma_{\text{po}}^{sj}) \quad (6)$$

where σ_{po}^{sj} is the average pull-out stress due to the friction between the fibre pull-outs and can be calculated as

$$\sigma_{\text{po}}^{sj} = \frac{\tau_{\text{fr}} \cdot C_f}{n_{\text{el}}^{sj} \cdot A_f} \cdot \sum_{N_{\text{cl}}^{sj}} \min |j - j_{\text{fa}}| \cdot l_{\text{el}} \quad (7)$$

where τ_{fr} is the frictional stress acting on the lateral surface of each fibre pull-out and $\min |j - j_{\text{fa}}| \cdot l_{\text{el}}$ is the pull-out length ℓ_{po}^{ij} , which is the distance between the cross section j and the cross-section of the closest failed element j_{fa} in the same fibre i (see Figure 3c). The pull-out stress decreases the energy available for crack propagation, and reflects the fact that clusters of broken fibres which are almost coplanar are more likely to become critical than clusters which are more dispersed.

Hence, at each cross section j , Eqs.(5-7) are computed for each cluster of broken fibres, and a cluster criticality index I_{cl}^{sj} is defined:

$$I_{\text{cl}}^{sj} = \frac{a_{\text{eq}}^{sj}}{a_{\text{cr}}^{sj}} \quad (8)$$

If $I_{\text{cl}}^{sj} \geq 1$ for any cluster, it is assumed to propagate catastrophically and in consequence the bundle is considered failed.

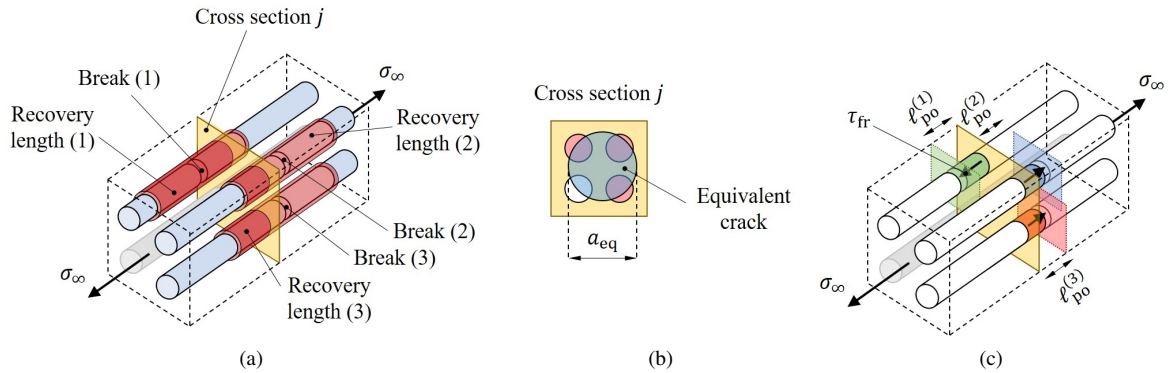


Figure 3 Fracture mechanics modeling. (a) Cluster of broken fibres. (b) Equivalent crack size. (c) Pull-out phenomenon (different colours were used for each fibre of the cluster).

C. Stress redistribution

Once the shear-lag stress limit is defined for each fibre, the final stress state in the bundle is computed by redistributing at each cross section the loss of stress from the saturated elements to the intact elements. Assuming that each cross section j contains \mathbb{N}_{st}^j saturated elements $(ij)_{\text{st}}$ and \mathbb{N}_{in}^j intact elements $(ij)_{\text{st}}$, the static equilibrium stress field σ^{ij} is computed applying the principle of superposition to each intact element:

$$\sigma^{ij} = \begin{cases} \sigma_{\text{sl}}^{ij} & \text{if } ij \in \mathbb{N}_{\text{st}}^j \\ \sigma_{\infty} + \sum_{\mathbb{N}_{\text{st}}^j} \Delta\sigma^{(ij)_{\text{in}}(ij)_{\text{st}}} & \text{if } ij \in \mathbb{N}_{\text{in}}^j \end{cases} \quad (9)$$

where $\Delta\sigma^{(ij)_{\text{in}}(ij)_{\text{st}}}$ is the additional stress redistributed on $(ij)_{\text{in}}$ as a result of the stress loss on $(ij)_{\text{st}}$.

Almost the totality of the FBMs in the literature only consider static equilibrium stress fields but, in reality, when a fibre fails, the stored elastic energy is released in form of a dynamic stress wave. This wave propagates throughout the intact fibres during a short time interval (hereafter *transient* interval), causing a dynamic stress redistribution σ_{dyn}^{ij} , and then is dampened by the material and the field reverts to equilibrium (σ^{ij}).

Considering that dynamic effects act by increasing the stress concentration on the intact fibres during the transient interval, the dynamic stresses can be computed from the static one with a dynamic magnification factor λ_{dyn} :

$$\sigma_{\text{dyn}}^{ij} = \begin{cases} \sigma_{\text{sl}}^{ij} & \text{if } ij \in \mathbb{N}_{\text{st}}^j; \\ \sigma_{\infty} + \lambda_{\text{dyn}} \cdot \sum_{\mathbb{N}_{\text{st}}^j} \Delta\sigma^{(ij)_{\text{in}}(ij)_{\text{st}}} & \text{if } ij \in \mathbb{N}_{\text{in}}^j. \end{cases} \quad (10)$$

The static equilibrium solution is given when $\lambda_{\text{dyn}} = 1$, but the fibres experience higher stress levels during the dynamic transient. Dynamic stress concentrations have been reported to range between 160% and 200% of the corresponding static ones depending on the material properties and fibre packing.^{9,20,27-30} However, in this model we do not seek to simulate the stress evolution during the entire transient, but we estimate an upper-bound of the dynamic effects. Hence, we assume a maximum dynamic magnification factor of $\lambda_{\text{dyn}} = 2$, since this is the theoretical maximum magnification for a spring-mass system without damping subject to a step load. Comparing Eq.(10) with $\lambda_{\text{dyn}} = 2$ with Eq.(9) will reveal an upper-bound for the role of dynamic stresses in comparison with static levels.

To calculate each $\Delta\sigma^{(ij)_{\text{in}}(ij)_{\text{st}}}$, we propose an analytical power law to reproduce the fact that the closer regions to broken fibres undergo higher stresses than more distant ones:

$$\Delta\sigma^{(ij)_{\text{in}}(ij)_{\text{st}}} = \Phi^{(ij)_{\text{st}}} \cdot \left(\frac{r^{(ij)_{\text{in}}(ij)_{\text{st}}}}{s} \right)^{-\gamma}, \quad (11)$$

where $r^{(ij)_{\text{in}}(ij)_{\text{st}}}$ is the distance between fibre elements in the cross section j and is normalized by fibre spacing s (hereafter indicated as $\bar{r}^{\text{in,st}}$), and γ is the parameter which controls the shape of the stress redistribution function. The variable $\Phi^{(ij)_{\text{st}}}$ is calculated by imposing force equilibrium to the entire bundle cross section:

$$\sigma_{\infty} - \sigma_{\text{sl}}^{(ij)_{\text{st}}} = \sum_{\mathbb{N}_{\text{in}}^j} \Phi^{(ij)_{\text{st}}} \cdot \left(\bar{r}^{\text{in,st}} \right)^{-\gamma} \Rightarrow \Phi^{(ij)_{\text{st}}} = \frac{\sigma_{\infty} - \sigma_{\text{sl}}^{(ij)_{\text{st}}}}{\sum_{\mathbb{N}_{\text{in}}^j} \left(\bar{r}^{\text{in,st}} \right)^{-\gamma}}. \quad (12)$$

St-Pierre et al. developed a similar formulation for the stress redistribution around clusters of broken fibres¹³ and validated a value of $\gamma = 2$ for the redistribution function, which we will use for all the simulations throughout this document.

The additional stresses may cause new elements in the cross section j to reach their shear-lag limit (incrementing the set of saturated elements \mathbb{N}_{st}^j); in consequence, the calculation of the stress state in the bundle is performed iteratively. After the first step, Eqs.(9)-(12) are used but starting each iteration with the previous field σ^{ij} instead of σ_{∞} .

D. Failure process simulation

Under a certain remote stress σ_{∞} , the bundle status is defined by the cluster criticality indexes I_{cl}^{sj} , given by Eq.(8), and both the static and dynamic stress fields σ^{ij} and σ_{dyn}^{ij} , given by Eqs.(9) and (10). To simulate the entire failure

process and obtain the ultimate strength of the bundle X_b , we set an iterative process by varying $\sigma_\infty(t^k)$ ($t^k=0,1,2,\dots$) until final failure.

At each step t^k , only one new fibre element fails, which will be identified as $(ij)_{fa}(t^k)$, and the bundle status is recalculated for the damage status defined by all the fibre elements broken up to that point, under the asymptotic stress $\sigma_\infty(t^k)$. As initial condition to start the simulation ($t^k = 0$), the bundle is loaded to $\sigma_\infty(0) = \min(X^{ij})$ to break the weakest fibre element $(ij)_{fa}(0)$.

To select which element breaks at each step and how to update the remote stress, we consider that damage in the bundle can progress either through (i) fibre failure due to the dynamic stress concentrations during the transient interval, or (ii) fibre failure due to the rise of the asymptotic stress $\sigma_\infty(t^k)$.

Scenario (i) occurs if $\sigma_{dyn}^{ij}(t^k) \geq X^{ij}$ for at least one non-broken fibre element in the bundle. For all the elements that meet this condition, the new failed element $(ij)_{fa}(t^{k+1})$ is the closest to the last broken one. The asymptotic stress is updated as follows:

$$\sigma_\infty(t^{k+1}) = \sigma_\infty(t^k) \quad (13)$$

Scenario (ii) occurs if dynamic stress concentrations already dampened to the static levels without causing any new failure in the bundle. In this case, the asymptotic stress is raised to provoke the failure of the weakest non-broken element:

$$\sigma_\infty(t^{k+1}) = \min\left(\frac{X^{ij}}{\sigma_{ij}(t^k)}\right) \cdot \sigma_\infty(t^k) \quad (14)$$

The simulation is stopped if $I_{cl}^{sj}(t^k) \geq 1$ for any cluster and then $X_b = \sigma_\infty(t^k)$ (fracture mechanics driven failure); or if $\sigma^{ij}(t^k) \geq \sigma_{sl}^{ij}(t^k)$ for all the elements in the same cross section j , and then $X_b = \max(\sigma_\infty(t^k))$ (saturation of the shear-lag mechanism or strength of materials driven failure). The whole iterative procedure is summarized in Figure 4.

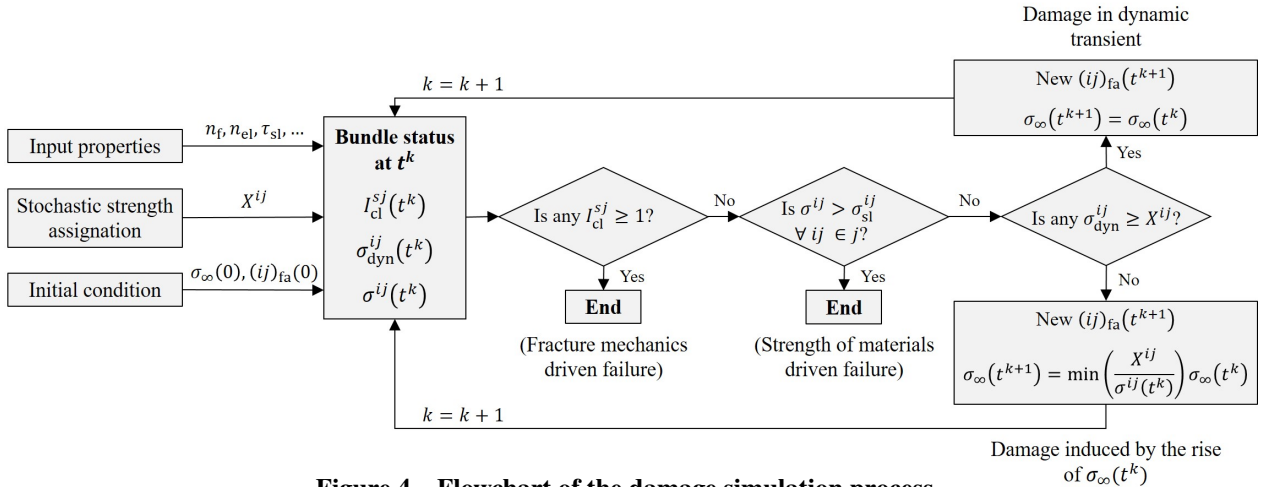


Figure 4 Flowchart of the damage simulation process.

E. Monte Carlo stopping criterion

To accurately calculate the statistical strength parameters (bundle mean strength \bar{X}_b and standard deviation SD_b), the selection of an appropriate number of Monte Carlo simulations is critical. Although most models in the literature use a fixed number of simulations for all bundle sizes, both experiments and models shows a decrease in the bundle strength variability when increasing the number of fibres in the bundle.^{11,31} In this work, a bundle-size variable number of Monte Carlo simulations was implemented as a way to increase computational efficiency, while keeping the accuracy of the results constant.

Given a sample with N simulations, and following the Central Value Theorem, it is possible to calculate the confidence interval at 95% as

$$w_{IC}^{95\%} = \left[\bar{X}_b^N - t(N-1, 0.025) \cdot \frac{SD_b^N}{\sqrt{N}}, \bar{X}_b^N + t(N-1, 0.025) \cdot \frac{SD_b^N}{\sqrt{N}} \right] \quad (15)$$

where $t(N - 1, 0.025)$ is the value of the Student's-t distribution with $N - 1$ degrees of freedom for a cumulative probability of 97.5%. The mean \bar{X}_b^N and standard deviation SD_b^N of the sample are used as estimators of the equivalent normal distribution parameters.

After each Monte Carlo simulation, Eq.(15) is computed until the width of the interval predicts the mean strength with a maximum accepted error $E_{\bar{X}} = \pm 1\%$. A minimum number of $N_{\min} = 12$ is used to assure that the initial estimation of the mean and standard deviation are statistically meaningful.

III. Results

Three different versions of the model are compared to analyse the features described above and capture the effects of each failure mechanism separately (Table 1). Model A correspond to a baseline version, which do not include dynamic effects (no dynamic stresses or $\lambda_{\text{dyn}} = 1$) nor fracture mechanics (infinite fracture toughness or $\lambda_{\text{fm}} = \infty$). Model B includes the effect of dynamic stress concentration factors in the predicted strength. Model C performs a parametric study with different values of λ_{fm} to study the scope of the fracture mechanics driven failure.

Unless otherwise stated, all the simulations were carried out with $l_{\text{el}} = 0.005$ mm and $l_s = 1$ mm (200 elements per fibre). Scaling from l_s to a different bundle length l_b is performed using the Weakest Link Theory (see Appendix A). No scaling is applied to the number of fibres, which means that the actually desired number of fibres is simulated directly.

Figure 5a shows the comparison between the predicted mean strength and coefficient of variation between models A and B, for length $l_b = 10$ mm. The nominal input properties for the fibres and resin were obtained from Okabe and Takeda¹² and listed in Table 2. Figure 5b shows how damage in the bundle varies when considering dynamic effects.

Figure 6a compares the mean strength and coefficient of variation between models A and C, for a bundle length $l_b = 10$ mm and the same input properties. To apply Eqs.(5)-(7) the composite mechanical properties are $E = 120$ GPa, $\nu = 0.28$ and $\tau_{\text{fr}} = 10$ MPa, while λ_{fm} is treated as a free parameter in the model and results for different values are presented. Figure 6b presents the impact of fracture mechanics in the maximum cluster size in the bundle.

Figures 7a-c validates the models against experimental strength data. Figures 7a-b shows predictions of Models A and B for micro-composites (four square-packed fibres). Fibre properties were taken from the experiments of Beyerlein and Phoenix,³¹ and two different matrices were compared: matrix (I) is a low modulus, flexible epoxy, with $\tau_{\text{sl}} = 3.96$ MPa and matrix (II) is a high modulus, stiff epoxy, with $\tau_{\text{sl}} = 41.67$ MPa. Both yield stresses were obtained from Netravali et al.³² In this case, no scaling technique is applied, so $l_s = l_b = 10$ mm. The strength predictions for the same material system obtained via Monte Carlo simulation of a full-field FE bundle model from St-Pierre et al.¹³ were included for comparison.

Figures 7c compares results from models A, B and C with experimental data for the average strength of composite bundles ranging from one thousand up to one million fibres obtained from Okabe and Takeda (input properties in Table 2). The results were scaled to $l_b = 10$ mm from the simulated bundle length $l_s = 1$ mm. For model C, results for different values of λ_{fm} are presented.

Table 1 Summary of the three models developed for comparison

Ref.	Model family	Dynamic stresses	Fracture mechanics
Model A	Baseline	$\lambda_{\text{dyn}} = 1$	$\lambda_{\text{fm}} = \infty$
Model B	Dynamic effects	$\lambda_{\text{dyn}} = 2$	$\lambda_{\text{fm}} = \infty$
Model C	Fracture mechanics	$\lambda_{\text{dyn}} = 1$	Parametric study

Table 2 Fibre and bundle input properties for the study

Reference	Fibre properties and Weibull parameters					Bundle inputs		
	Type	ϕ_f [μm]	X_0^l [MPa]	m [-]	l_f [mm]	τ_{sl} [MPa]	Packing	V_f [-]
Okabe and Takeda ¹²	T800H	5.0	3570	3.8	50	52.4	Square	0.60
Bayerlein and Phoenix ³¹	AS4	6.85	4493	4.8	10	3.96 / 41.67	Square	0.70

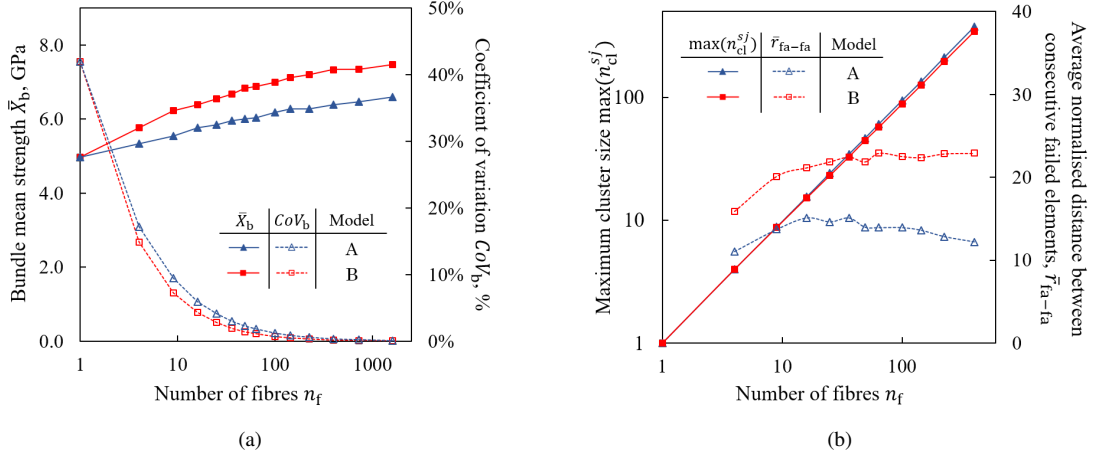


Figure 5 Role of dynamic effects. (a) Predicted strength and coefficient of variation for models A and B (Results presented for $l_b = 10\text{mm}$). (b) Effect of dynamic stress concentration in the formation of clusters.

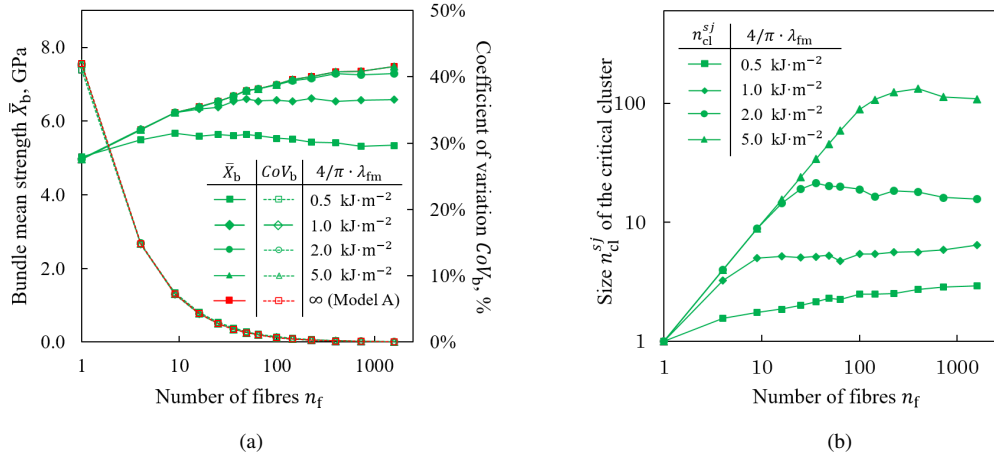


Figure 6 Role of fracture mechanics. (a) Predicted strength and coefficient of variation for models A and C (Results presented for $l_b = 10\text{mm}$ and for different values of λ_{fm}). (b) Critical cluster size as a function of the bundle size (for different values of λ_{fm}).

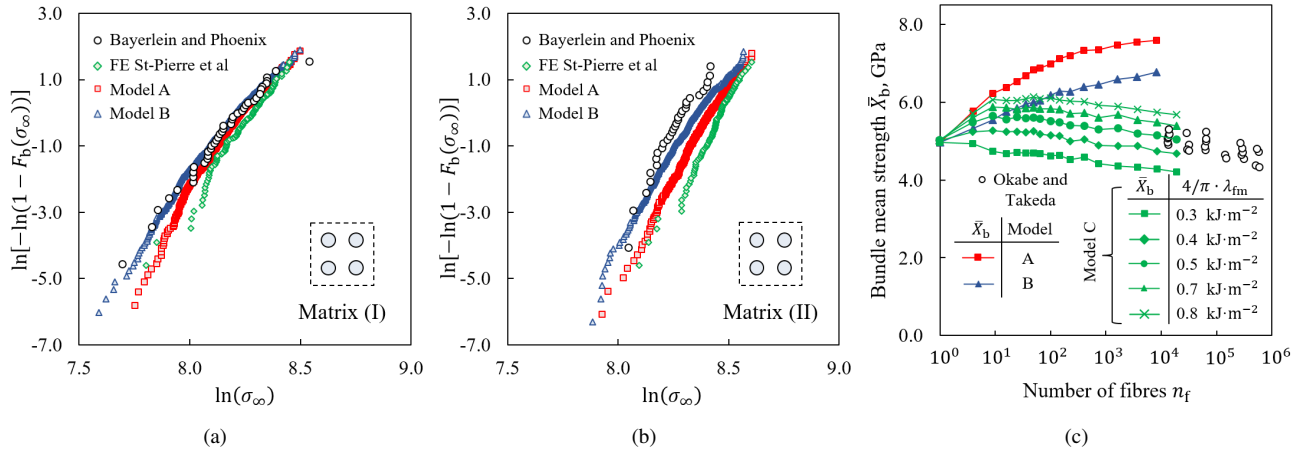


Figure 7 Validation against experimental data (all results presented for $l_b = 10\text{mm}$). (a)-(b) Predicted bundle strength distributions for micro-composites for matrices (I) and (II) (results presented on a Weibull plot; the geometry of the packing is depicted). (c) Predicted strength for macro-composites.

IV. Discussion

A. Dynamic effects

Figure 5a shows that both models A and B predict a constantly increasing bundle strength and a coefficient of variation that decreases substantially with bundle size, thus the selection of a bundle-size variable number of Monte Carlo simulations is proven to be a very effective approach. Dynamic effects act lowering the predicted bundle strength by around 10%, but the true effect is expected to be lower, since model B represent an upper-bound for the maximum intensity of these effects.

Dynamic stress concentrations do not change the maximum size of the clusters formed, but the average distance between consecutive failure points becomes smaller (Figure 5b), suggesting that dynamic effects lead to clusters that are more coplanar. The formation of coplanar clusters during tensile tests have been confirmed by computer tomography experiments,²⁰ and is a feature that static models struggle to represent correctly. Therefore, the lower bundle strength predicted with including dynamic effects appear to be the result of the higher stress concentrations and easier damage localization around clusters of broken fibres introduced by the dynamic effects.

B. Fracture mechanics

When a fracture mechanics failure criterion is considered, the predicted bundle strength decreases significantly (Figure 6a). Furthermore, lower values of λ_{fm} changes the overall size effects: strength presents a maximum for medium-size bundles (under 100 fibres) and then decreases with bundle size. The bundle variability is not affected by fracture mechanics.

Critical cluster sizes predicted by model C are much smaller than the maximum cluster sizes given by models A/B and appear to reach an horizontal asymptote, as opposed to the continuous growth shown by the models without fracture mechanics (Figure 6b). Although direct comparison with experimental results is not possible at this point, this result is in line with experimental evidence, which has not reported clusters greater than 14 fibres, even for large bundles.^{6,20} Other models in the literature which do not consider fracture mechanics also tend to severely overestimate the critical cluster size.⁶

C. Validation against micro-composites

The models correlate very well with the experimental data for matrix (I) (low modulus) and the predicted mean strengths do not deviate more than 2% (Figure 7a). The correlation with St-Pierre et al. FE data¹³ is also excellent. For matrix (II) (high modulus), predictions appear to overestimate slightly the experimental strength, but they are still very close to FE data (Figure 7b). It should be noted that Netravali et al.³² have reported the occurrence of debonding at the fibre matrix interface during single fibre fragmentation tests with matrix (II), while no debonding was observed for the flexible matrix (I). Debonding at the fibre matrix interface results in a longer recovery length and this may lower the bundle strength, so this consideration may explain why the simulations tend to overestimate the experimental results.

D. Validation against macro-composites

It is observed in Figure (Figure 7c) that both models A and B overestimate the strength of large bundles. Furthermore, the size effect (decrease in strength with the number of fibres in the bundle) observed in the range of the experiments cannot be reproduced by any of the two models, which both exhibit a positive trend for the bundle strength. These results suggest that the strength of large composite bundles, and in particular the size effects, cannot be correctly predicted considering only strength of materials as the failure theory (even in the case of dynamic stress concentration).

In contrast, predictions for model C for the values of λ_{fm} studied are in the same range of the experimental results. Additionally, the reduction in the predicted mean strength with the bundle size is compatible with the trend of the experimental data. Note that, although predictions depend on λ_{fm} , treated as a free parameter of the model at this point, the model predicts the correct size effect for all the values considered. This suggest that failure in large composite bundles may be driven by fracture mechanics.

V. Conclusion

A family of semi-analytical fibre bundle models was developed to efficiently simulate the longitudinal tensile failure of large composite bundles. A field superposition method was implemented to calculate the stress concentrations and capture the effect of clusters of broken fibres in the shear-lag recovery mechanism. A bundle-size dependent variable number of Monte Carlo simulations was implemented, resulting in a great improvement of the computational efficiency and allowing the direct simulation of bundle sizes up to thousands of fibres.

The models include both strength of materials and fracture mechanics as bundle failure theories. Additionally, a formulation to investigate the effect of dynamic stress concentrations on the failure process was included. To the knowledge of the authors, it is the first time in the literature that dynamic effects and fracture mechanics are investigated through direct simulation in a fibre bundle model.

All the models of the family exhibit a generally good correlation with experimental strength distributions for micro-bundles. However, when considering experimental data for large bundles, results are severely overestimated if only strength of materials driven failure is considered, even considering dynamic effects that shows a maximum reduction possible of about 10% in the predicted bundle strength. The addition of the fracture mechanics failure criterion allows the prediction of lower values with a negative trend for the strength of large bundles, in addition to a smaller cluster size which stays rather constant even for large bundles. Both considerations are in agreement with experimental evidence and suggest that fracture mechanics may be the physical mechanism necessary to reproduce the size effect in large composite bundles. This is arguably the most important outcome of this work.

Appendix

A. Assignment of stochastic strength and scaling

The Weibull distribution³³ is widely adopted in the literature to model the stochastic variability of the strength in composite fibres.^{11,13,14,16,34–36} For a single fibre with reference length l_r , the Weibull strength distribution is defined by the shape parameter m^{l_r} and the scale parameter $X_0^{l_r}$. The failure probability F of a fibre with length l_r under a remote stress σ_∞ is:

$$F(\sigma_\infty) = 1 - S(\sigma_\infty) = 1 - \exp\left(-\frac{\sigma_\infty}{X_0^{l_r}}\right)^{m^{l_r}} \quad (\text{A1})$$

where $S(\sigma_\infty)$ is the survival probability under the remote stress σ_∞ .

The Weakest Link Theory,^{5,37} which states that a chain of n elements survives under a remote stress σ_∞ only if each of the elements survives under σ_∞ , is used to scale the Weibull parameters from the reference length l_r to a length l :

$$m^l = m^{l_r}; \quad X_0^l = X_0^{l_r} \cdot \left(\frac{l_r}{l}\right)^{1/m^{l_r}} \quad (\text{A2})$$

We used this formulation to assign a random strength X^{ij} to each fibre element of length l_{el} in the bundle. Combining Eqs.(A1-A2) and assigning a random survival probability with a random number S^{ij} :

$$X^{ij} = X_0^{l_r} \cdot \left(-\frac{l_r}{l_{el}} \cdot \ln S^{ij}\right)^{1/m^{l_r}} \quad (\text{A3})$$

The same formulation is used to scale the results from a simulation bundle length l_s to another bundle length l_b . Being $X_b^1 \leq X_b^2 \leq \dots \leq X_b^N \dots \leq X_b^{N_{MC}}$ the predicted bundle strengths corresponding to each one of the N_{MC} Monte Carlo simulations for a bundle of length l_s , the cumulative distribution function for the bundle strength is obtained assigning a bundle failure probability F_b to each of the N_{MC} Monte Carlo strengths:

$$F_b^N = (N - 1)/N_{MC} \quad (\text{A4})$$

This distribution is fitted using a Weibull distribution with parameters m^{l_s} and $X_0^{l_s}$ that correspond to its mean strength $X_b^{l_s}$ and standard deviation $SD_b^{l_s}$. Then, the parameters are scaled to l_b following Eq.(A2).

Acknowledgments

I would like to extend my gratitude to Dr Soraia Pimenta, who continually revised the content of this paper and made several contributions that improved the quality of the work.

References

- [1] Wisnom, M. R., "Size effects in the testing of fibre-composite materials," *Compos. Sci. Technol.*, Vol. 59, No. 13, 1999, pp. 1937–1957.
- [2] Bažant, Z. P., "Size effect on structural strength: a review," *Arch. Appl. Mech.*, Vol. 69, No. 9-10, 1999, pp. 703–725.

- [3] Xu, X., Wisnom, M. R., Mahadik, Y., and Hallett, S. R., “An experimental investigation into size effects in quasi-isotropic carbon/epoxy laminates with sharp and blunt notches,” *Compos. Sci. Technol.*, Vol. 100, 2014, pp. 220–227.
- [4] Xu, X., Wisnom, M. R., Li, X., and Hallett, S. R., “A numerical investigation into size effects in centre-notched quasi-isotropic carbon/epoxy laminates,” *Compos. Sci. Technol.*, Vol. 111, 2015, pp. 32–39.
- [5] Pimenta, S., “Fibre failure modelling,” *Numerical Modelling of Failure in Advanced Composite Materials*, edited by P. P. Camanho and S. R. Hallett, 2015, pp. 193–224.
- [6] Swolfs, Y., Pimenta, S., Thionnet, A., Bunsell, A., Gorbatikh, L., Morton, H., Sinclair, I., and Spearing, M., “A benchmarking exercise for three longitudinal strength models for unidirectional fibre-reinforced composites,” *Proceedings of ICCM-21. Xi’an, China*, 2017.
- [7] Landis, C. M., Beyerlein, I. J., and McMeeking, R. M., “Micromechanical simulation of the failure of fiber reinforced composites,” *J. Mech. Phys. Solids*, Vol. 48, No. 3, 2000, pp. 621–648.
- [8] Curtin, W. A., and Takeda, N., “Tensile Strength of Fiber-Reinforced Composites: I. Model and Effects of Local Fiber Geometry,” *J. Compos. Mater.*, Vol. 32, No. 22, 1998, pp. 2042–2059.
- [9] Hedgepeth, J. M., “Stress Concentrations in Filamentary Structures,” *NASA technical report*, 1961.
- [10] Rosen, B. W., “Tensile Failure of Fibrous Composites,” *AIAA JOURNAL*, Vol. 2, No. 11, 1964, pp. 1985–1991.
- [11] Pimenta, S., and Pinho, S. T., “Hierarchical scaling law for the strength of composite fibre bundles,” *J. Mech. Phys. Solids*, Vol. 61, No. 6, 2013, pp. 1337–1356.
- [12] Okabe, T., “Size effect on tensile strength of unidirectional CFRP composites—experiment and simulation,” *Compos. Sci. Technol.*, Vol. 62, No. 15, 2002, pp. 2053–2064.
- [13] St-Pierre, L., Martorell, N. J., and Pinho, S. T., “Stress redistribution around clusters of broken fibres in a composite,” *Compos. Struct.*, Vol. 168, 2017, pp. 226–233.
- [14] Okabe, T., Sekine, H., Ishii, K., Nishikawa, M., and Takeda, N., “Numerical method for failure simulation of unidirectional fiber-reinforced composites with spring element model,” *Compos. Sci. Technol.*, Vol. 65, No. 6, 2005, pp. 921–933.
- [15] Zhou, S. J., and Curtin, W. A., “Failure of fiber composites: A lattice green function model,” *Acta Metall. Mater.*, Vol. 43, No. 8, 1995, pp. 3093–3104.
- [16] Swolfs, Y., McMeeking, R. M., Verpoest, I., and Gorbatikh, L., “Matrix cracks around fibre breaks and their effect on stress redistribution and failure development in unidirectional composites,” *Compos. Sci. Technol.*, Vol. 108, 2015, pp. 16–22.
- [17] Bazant, Z. P., Daniel, I. M., and Li, Z., “Size effect and fracture characteristics of composite laminates,” *of the ASME*(. . . , 1996.
- [18] Aroush, D. R.-B., Maire, E., Gauthier, C., Youssef, S., Cloetens, P., and Wagner, H. D., “A study of fracture of unidirectional composites using in situ high-resolution synchrotron X-ray microtomography,” *Compos. Sci. Technol.*, Vol. 66, No. 10, 2006, pp. 1348–1353.
- [19] Scott, A. E., Mavrogordato, M., Wright, P., Sinclair, I., and Spearing, S. M., “In situ fibre fracture measurement in carbon–epoxy laminates using high resolution computed tomography,” *Compos. Sci. Technol.*, Vol. 71, No. 12, 2011, pp. 1471–1477.
- [20] Swolfs, Y., Verpoest, I., and Gorbatikh, L., “A review of input data and modelling assumptions in longitudinal strength models for unidirectional fibre-reinforced composites,” *Compos. Struct.*, Vol. 150, 2016, pp. 153–172.
- [21] Bullegas, G., Lamela, J. M., Pinho, S. T., and Pimenta, S., “On the roles of dynamic stress concentrations and fracture mechanics in the longitudinal tensile failure of fibre-reinforced composites,” *In preparation for publication on the Journal of the Mechanics and Physics of Solids*, 2018.
- [22] Romanov, V., Lomov, S. V., Swolfs, Y., Orlova, S., Gorbatikh, L., and Verpoest, I., “Statistical analysis of real and simulated fibre arrangements in unidirectional composites,” *Compos. Sci. Technol.*, Vol. 87, No. Supplement C, 2013, pp. 126–134.
- [23] Kelly, A., and Tyson, W. R., “Tensile properties of fibre-reinforced metals: Copper/tungsten and copper/molybdenum,” *J. Mech. Phys. Solids*, Vol. 13, No. 6, 1965, pp. 329–350.
- [24] Landis, C. M., and McMeeking, R. M., “A shear-lag model for a broken fiber embedded in a composite with a ductile matrix,” *Compos. Sci. Technol.*, Vol. 59, No. 3, 1999, pp. 447–457.
- [25] Nairn, J. A., “Fracture Mechanics of Unidirectional Composites Using the Shear-Lag Model II: Experiment,” *J. Compos. Mater.*, Vol. 22, No. 6, 1988, pp. 589–600.
- [26] Nairn, J. A., “Fracture Mechanics of Unidirectional Composites Using the Shear-Lag Model I: Theory,” *J. Compos. Mater.*, Vol. 22, No. 6, 1988, pp. 561–588.
- [27] Sakharova, E. N., and Ovchinskii, A. S., “Dynamics of stress redistribution in a ruptured fiber of a composition material,” *Mech. Compos. Mater.*, Vol. 15, No. 1, 1979, pp. 45–51.
- [28] Ganesh, R., Sockalingam, S., (Gama) Haque, B. Z., and Gillespie, J. W., “Dynamic effects of single fiber break in unidirectional glass fiber-reinforced composites,” *J. Compos. Mater.*, Vol. 51, No. 9, 2016, pp. 1307–1320.
- [29] Sakharova, E. N., and Ovchinskii, A. S., “Influence of dynamic effects accompanying rupture of fibers and separation of fibers from the matrix on interaction between failure micromechanisms of composite materials,” *Mech. Compos. Mater.*, Vol. 20, No. 3, 1984, pp. 323–327.
- [30] Xing Ji, Liu, X.-R., and Chou, T.-W., “Dynamic Stress Concentration Factors in Unidirectional Composites,” *J. Compos. Mater.*, Vol. 19, No. 3, 1985, pp. 269–275.
- [31] Beyerlein, I. J., and Phoenix, S. L., “Statistics for the strength and size effects of microcomposites with four carbon fibers in epoxy resin,” *Compos. Sci. Technol.*, Vol. 56, No. 1, 1996, pp. 75–92.
- [32] Netravali, A. N., Henstenburg, R. B., Phoenix, S. L., and Schwartz, P., “Interfacial shear strength studies using the single-filament-composite test. I: Experiments on graphite fibers in epoxy,” *Polym. Compos.*, Vol. 10, No. 4, 1989, pp. 226–241.
- [33] Weibull, G. W., “A statistical distribution function of wide applicability,” *J. Appl. Math.*, 1951, pp. 293–297.
- [34] Swolfs, Y., Verpoest, I., and Gorbatikh, L., “Issues in strength models for unidirectional fibre-reinforced composites related to Weibull distributions, fibre packings and boundary effects,” *Compos. Sci. Technol.*, Vol. 114, No. Supplement C, 2015, pp. 42–49.
- [35] Okabe, T., Takeda, N., Kamoshida, Y., Shimizu, M., and Curtin, W. A., “A 3D shear-lag model considering micro-damage and statistical strength prediction of unidirectional fiber-reinforced composites,” *Compos. Sci. Technol.*, Vol. 61, No. 12, 2001, pp. 1773–1787.
- [36] Curtis, P. T., “A Computer Model of the Tensile Failure Process in Unidirectional Fibre Composites,” *Compos. Sci. Technol.*, Vol. 27, 1986, pp. 63–86.
- [37] Peirce, F. T., “Tensile tests for cotton yarns: “the weakest link” theorems on the strength of long and of composite specimens,” *J. Text. Inst.*, Vol. 17, 1926, pp. T355–368.